

Model-Agnostic, Temperature-Informed Sampling Enhances Cross-Year Crop Mapping with Deep Learning

Mehmet Ozgur Turkoglu, Sélène Ledain, Helge Aasen

Earth Observation of Agroecosystems, Agroscope, Switzerland
{mehmet.tuerkoglu, selene.ledain, helge.aasen}@agroscope.admin.ch

Keywords: Crop Mapping, Deep Learning, Transformer, Temperature Data, Time Series, Uncertainty Quantification

Abstract

Conventional benchmarks for crop type classification from optical satellite time series typically assume access to labeled data from the same year and rely on fixed calendar-day sampling. This limits generalization across seasons, where crop phenology shifts due to interannual climate variability, and precludes real-time application when current-year labels are unavailable. Furthermore, uncertainty quantification is often neglected, making such approaches unreliable for crop monitoring applications. Inspired by ecophysiological principles of plant growth, we propose a simple, model-agnostic sampling strategy that leverages growing degree days (GDD), based on daily average temperature, to replace calendar time with thermal time. By uniformly subsampling time series in this biologically meaningful domain, the method emphasizes phenologically active growth stages while reducing temporal redundancy and noise. We evaluate the method on a multi-year Sentinel-2 dataset spanning all of Switzerland, training on one growing season and testing on other seasons. Compared to state-of-the-art baselines, our method delivers substantial gains in classification accuracy and, critically, produces more calibrated uncertainty estimates. Notably, our method excels in low-data regimes and enables significantly more accurate early-season classification. With only 10 percent of the training data, our method surpasses the state-of-the-art baseline in both predictive accuracy and uncertainty estimation, and by the end of June, it achieves performance similar to a baseline trained on the full season. These results demonstrate that leveraging temperature data not only improves predictive performance across seasons but also enhances the robustness and trustworthiness of crop-type mapping in real-world applications.

1. Introduction

Monitoring agricultural land use is crucial for the sustainability of our food systems (Gómez et al., 2016). As the world’s population grows, climates shift, and diets evolve, there is a pressing need for monitoring tools that deliver reliable, affordable, and scalable insights into farming practices. In contrast to traditional methods, such as field surveys and self-reported data, which can be labor-intensive, expensive, and susceptible to errors, remote sensing-based approaches offer a faster, more cost-effective, and less subjective alternative for tracking land-use dynamics (Weiss et al., 2020).

Recent progress in remote sensing technologies and machine learning algorithms has significantly enhanced the ability to monitor agricultural land use. High-resolution, multi-spectral data from platforms such as Sentinel-2 provide frequent, detailed observations of croplands at minimal cost. By applying advanced machine learning methods, including conventional ensemble learners, e.g. XGBoost (Chen and Guestrin, 2016) and deep neural networks, e.g. Transformers (Vaswani et al., 2017), to these time series images, we can capture crop-specific growth dynamics and distinguish among diverse management practices with high precision. These integrated approaches enable automated, scalable mapping of crop types and growth stages, supporting timely, data driven decisions for sustainable agriculture (Turkoglu, 2023).

Modern deep learning methods (Garnot and Landrieu (2021), Turkoglu et al. (2021a), Metzger et al. (2021), Tarasiou et al. (2023), Rußwurm and Körner (2018)) excel in classifying crop types from optical satellite image time series. However, these models are typically trained on curated datasets with limited

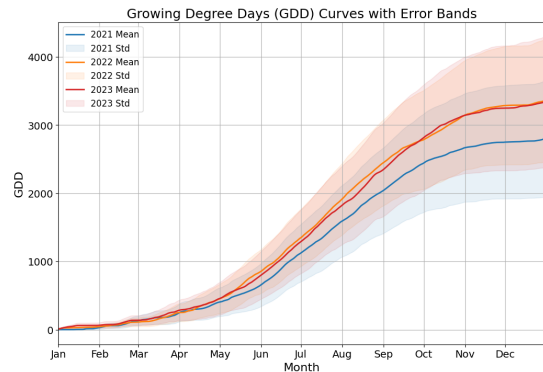


Figure 1. Cumulative Growing Degree Days (GDD) across Switzerland for multiple years.

size and/or validated on data collected within a single growing season (Rußwurm et al. (2019), Garnot and Landrieu (2021), Schneider et al. (2023), Turkoglu et al. (2021a)), neglecting interannual shifts in growth driven by climate variability and thus limiting their applicability across years and regions. Furthermore, their dependence on current-year labeled data for training precludes real time deployment during the ongoing season. As also noted by Roscher et al. (2024), model development should focus on datasets with real-world relevance to further improve accuracy, generalization ability, and real impact on end user applications. Lastly, although these approaches may achieve state-of-the-art accuracy, they rarely incorporate uncertainty quantification, leaving predictive confidence unassessed and often uncalibrated. Ensuring the models are well-calibrated makes them reliable components of agricultural monitoring systems, where

miscalibration could otherwise lead to costly resource misallocations or risk mismanagement.

Seen from an ecophysiological point of view, crop development is majorly driven by thermal conditions, since temperature plays a pivotal role in determining growth and phenological development. Temperature can vary substantially year-to-year within the same region or across different regions, as illustrated in Figure 1. It shows how the annual cumulative daily temperature in Switzerland varies between seasons. Similarly, Figure 2 (left) depicts Normalised Difference Vegetation Index (NDVI) time series for a single field over two years, revealing a noticeable shift in the crop’s growth trajectory despite the crop type remaining constant. Also see Figure 3, which illustrates how the same agricultural landscape can appear markedly different in satellite imagery across different years. By expressing crop development relative to a thermal time calendar, using growing degree days (GDD) rather than calendar days, the apparent interannual mismatch in growth cycles becomes significantly less pronounced (Figure 2 (right)). This motivates integrating temperature-based normalization into crop monitoring workflows to enhance model robustness and generalization across years. While other environmental drivers like precipitation undoubtedly influence crop growth, their incorporation falls beyond the scope of this study and is reserved for future research.

In this work, we build upon the state-of-the-art attention-based deep learning architecture proposed by Garnot and Landrieu (2021), and introduce a simple, model-agnostic sampling strategy that incorporates daily average temperature to reduce redundancy and noise in satellite image time series. Deep learning models for crop classification typically rely on subsampled time series, as crop development progresses gradually and many satellite observations are temporally redundant. Subsampling is also necessary to reduce sequence length for efficient model training and inference within limited GPU memory. To better guide this selection, we replace calendar days with growing degree days (GDD) as the temporal reference and perform uniform subsampling in this thermal time domain. This approach emphasizes the crop’s biologically active periods, ensuring that the model focuses on the most informative observations.

We evaluate our GDD-informed sampling approach on a multi-year, country-wide dataset spanning three Swiss growing seasons by training on one year and testing on the other two. We benchmark against state-of-the-art baselines, evaluate low-data scenarios using just 10% of training samples, assess early-season classification performance, and examine uncertainty calibration for reliable decision support. We hypothesize that GDD-informed sampling will boost both classification accuracy and uncertainty estimation, also including under data scarcity and in early-growth phases, thereby addressing critical robustness and timeliness challenges in operational crop monitoring.

In summary, our contributions are as follows:

- We introduce a simple yet effective model-agnostic approach that takes into account ecophysiological principles of plant growth: Thermal-Time-based Temporal Sampling (T3S), which allows integration of temperature data into any deep learning model, irrespective of model architecture.
- We benchmark the T3S approach to other state-of-the-art approaches. The results demonstrate substantial improve-

ments in predictive accuracy and uncertainty quantification across extensive country-wide, cross-year experiments, including low-data regimes and early-season classification settings.

- We publicly release the SwissCrop dataset, a comprehensive, multi-year crop dataset, along with code to support further research and facilitate seamless integration into deep learning workflows.

2. Related Work

Deep Learning for Crop Mapping from Satellite Imagery.

Deep learning has dramatically improved crop-type classification from satellite time series, outperforming traditional methods based on handcrafted features (Turkoglu, 2023). Early sequence-modeling approaches used recurrent architectures to capture phenological dynamics. Long short-term memory (LSTM) networks demonstrated strong performance on multi-temporal inputs (Rußwurm and Körner, 2017), and the convolutional-RNN (convRNN) version further boosted both accuracy and efficiency (Turkoglu et al., 2021a).

Attention mechanisms have emerged as a powerful alternative for modeling long-range temporal dependencies. Rußwurm and Körner (2020) and Garnot et al. (2020) were the first to apply self-attention to crop classification from Sentinel-2 data and showed improved results. Series (2020) then proposed the lightweight Temporal Attention Encoder (L-TAE), and Garnot and Landrieu (2021) embedded L-TAE within a U-Net backbone to adaptively weigh temporal features across space and time. More recently, fully attention-based Vision Transformer (ViT) adaptations have been explored for crop mapping (Bai et al., 2023), and Qin et al. (2024) leveraged the recently proposed Mamba state-space architecture to improve spatio-temporal classification performance.

To incorporate domain knowledge in deep learning architectures, several works introduce structured priors and hierarchical labels. Turkoglu et al. (2024b) exploited multi-scale crop class hierarchies within a parameter-efficient convRNN (i.e. convSTAR (Turkoglu et al., 2021b)) framework, and prototype-based supervision has been used to integrate class relationships into metric learning (Sainte Fare Garnot and Landrieu, 2020). Positional encodings tailored to agricultural cycles have also been proposed: (Nyborg et al., 2022) introduced thermal-time encoding, using cumulative growing degree days, to normalize phenological shifts across regions. This is the most relevant research for this paper. Moreover, practical deployment demands handling early-season data and irregular revisit intervals. Rußwurm et al. (2023) added an early classification reward loss to LSTM training, improving accuracy in the season when only partial time series are available. Metzger et al. (2021) leveraged neural ordinary differential equations (NODE) to process noisy and irregularly sampled time series, and Cai et al. (2023)’s collect–update–distribute design further addresses sampling irregularity.

Multi-Year Crop Mapping from Satellite Imagery. Multi-year crop mapping faces challenges due to temporal domain shifts such as interannual variability in weather, phenological differences, and sensor calibration issues. These factors often degrade the performance of models trained on single-season data when applied across multiple years. Turkoglu et al. (2024a) extended the experiments of Turkoglu et al. (2021a) to a multi-year setting, training and testing on data from two different

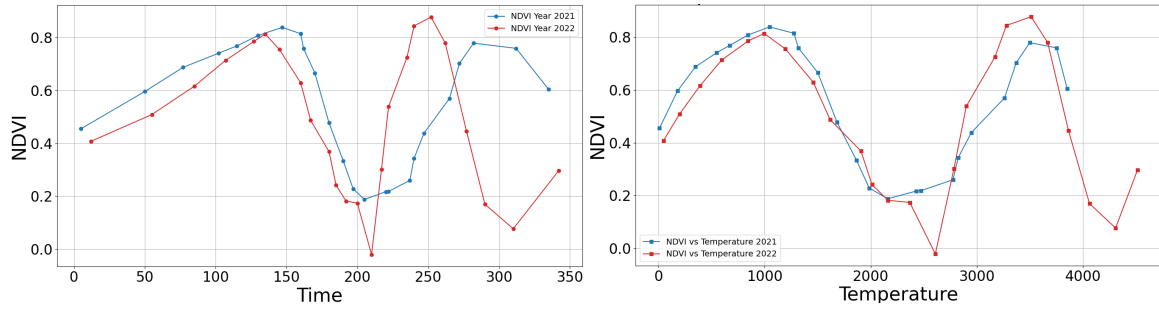


Figure 2. NDVI time series of two parcels with the same crop rotation over two years (2021 and 2022), aligned by calendar date (left) and by cumulative growing degree days (GDD) (right).

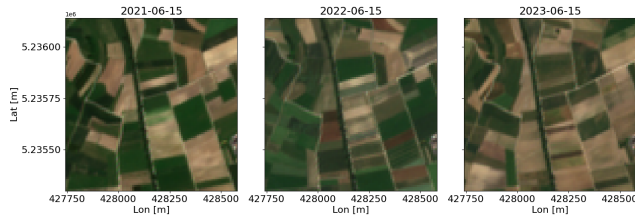


Figure 3. Year-to-year variation of the same agricultural landscape on June 15th from 2021 to 2023.

years, and reporting preliminary results. Blickensdörfer et al. (2022) employed a Random Forest classifier using dense Sentinel-2 and Landsat-8 time series, monthly Sentinel-1 composites, and environmental variables to evaluate the relative contributions of optical, radar, and environmental data across three meteorologically distinct years (2017–2019). Dubrovin et al. (2024) demonstrated that reconstructing multi-year Sentinel-2 NDVI time series with Fourier-based fitting and applying Gradient Boosting enables improved crop mapping across different years. Gao et al. (2023) investigated ways to optimize the use of multi-year samples in a within-season crop classification model. Qi et al. (2024) presented a Google Earth Engine workflow that fuses field-sample data with multi-year Sentinel-2 time series to map cropping systems on smallholder farms, achieving consistently robust results across diverse landscapes. Li et al. (2023) benchmarked deep learning segmentation models (e.g., U-Net and SegFormer (Xie et al., 2021)) for crop mapping across multiple years, while Sykas et al. (2022) evaluated convLSTM and convSTAR (Turkoglu et al., 2021b) networks in a similar multi-year context. Very recently, Khallaghi et al. (2025) shows improved results for cross-year crop mapping combining a U-Net with photometric augmentation, Tversky-Focal loss, and Monte Carlo (MC) Dropout.

Uncertainty Modeling in Deep Learning. Predictive uncertainty is commonly split into aleatoric uncertainty, which stems from inherent data variability such as class overlap or sensor noise, and epistemic uncertainty, which reflects model weight uncertainty due to insufficient coverage of the input space (Kendall and Gal, 2017). Exact Bayesian inference in deep networks is generally intractable, leading to approximate methods like variational inference (e.g., Bayes by Backprop, Blundell et al. 2015), Markov Chain Monte Carlo techniques such as Stochastic Gradient Langevin Dynamics (Welling and Teh, 2011). However, these approaches often struggle to scale to large architectures (Gustafsson et al., 2019). Probabilistic ensembles, particularly deep ensembles, currently represent the gold standard for epistemic uncertainty estimation in deep networks, providing well-calibrated and robust predictions by aggregating out-

puts from multiple independently trained models (Lakshminarayanan et al., 2017). However, the need to train and store several large networks incurs substantial computational and memory overhead. To address this, implicit ensemble techniques, such as Monte Carlo (MC) Dropout (Gal and Ghahramani, 2016), Snapshot Ensembles (Huang et al., 2017), Masksembles (Durosov et al., 2021), and FiLM-Ensemble (Turkoglu et al., 2022), approximate ensemble diversity via stochastic weight perturbations or dynamic weight combinations, significantly reducing resource requirements. Despite these gains in efficiency, implicit methods generally underperform full ensembles in both predictive accuracy and uncertainty calibration. More recently, LoRA-Ensemble has been introduced as a parameter-efficient alternative for transformer-based architectures, achieving uncertainty estimates competitive with deep ensembles at a fraction of the cost (Mühlematter et al., 2024).

Uncertainty Modeling in Satellite Imagery and Crop Mapping Uncertainty quantification has become a standard component of satellite-based land-cover and crop-mapping workflows, as it provides essential information for risk-aware decision-making in agricultural management and ecosystem monitoring. Generating per-pixel or per-field uncertainty maps alongside deterministic predictions enables practitioners to identify low-confidence areas and tailor downstream analyses accordingly. For example, Lang et al. (2022) employs a deep ensemble of convolutional neural networks to estimate global canopy height from sparse LiDAR samples and multi-sensor satellite imagery, producing uncertainty intervals that reflect both model and data variability. Becker et al. (2023) extends this ensemble approach to country-scale forest structure estimation at 10m resolution, demonstrating that dense uncertainty fields help flag regions where auxiliary field data are most needed.

In the context of crop yield and type mapping, several recent studies have adopted stochastic inference techniques. Tian et al. (2024) introduces an attention-guided multi-level crop network for winter wheat yield estimation at the county scale, applying MC Dropout during inference to derive spatially explicit uncertainty maps of yield forecasts. Similarly, Khallaghi et al. (2025) leverages MC Dropout in a U-Net segmentation framework to quantify per-pixel uncertainty in annual cropland masks across multiple years in Ghana, using the resulting confidence estimates to discard unreliable predictions. Liu et al. (2024) integrates MC Dropout in a ViT-ResNet feature encoder to produce field-level uncertainty scores, filtering out low-confidence labels to improve overall mapping precision. Beyond dropout-based methods, Baumert et al. (2024) proposes a probabilistic crop-type mapping method in which an ensemble of classifiers, each trained with perturbed inputs and hyperparameters on Sentinel-1, Sentinel-2, and Landsat-8 data, generates multiple

crop maps over Germany; per-pixel frequency counts across the ensemble yield robust probability distributions and uncertainty metrics. Maleki et al. (2024) refines the 30m cropland data by harnessing its built-in Random Forest confidence layer: low-certainty regions are iteratively reclassified using targeted ancillary datasets, resulting in a more accurate and self-aware mapping product. Collectively, these approaches demonstrate the critical role of uncertainty modeling in improving the reliability and interpretability of satellite-driven crop and canopy mapping systems.

3. Method

Our method builds on the U-Net with Temporal Attention Encoder (U-TAE) (Ronneberger et al., 2015; Garnot and Landrieu, 2021), a state-of-the-art deep learning model for dense segmentation of satellite image time series. Prior to presenting our sampling approach, we examine U-TAE on a standardized benchmark by adjusting sequence lengths and positional encodings to identify the minimal temporal resolution and ordering information needed for high classification accuracy. These insights directly inform our design choices and motivate the development of Thermal-Time-based Temporal Sampling (T3S), a model-agnostic method that aligns input selection with crop physiology.

3.1 U-Net with Temporal Attention Encoder (U-TAE)

The U-TAE model is a spatio-temporal neural network designed to extract dense and temporally-aware features from satellite image time series. It consists of a shared 2D convolutional encoder applied to each timestamp independently, followed by a temporal self-attention module that aggregates the encoded features across time. This attention module uses positional encoding to preserve temporal ordering and applies scaled dot-product attention to dynamically weigh each timestamp based on its relevance. The aggregated multi-temporal representation is then decoded through a U-Net-style decoder with skip connections, enabling high-resolution semantic segmentation. The architecture can handle variable-length input sequences and produce temporally adaptive representations of land cover. Refer to Garnot and Landrieu (2021) for more details.

3.2 Preliminary Analysis with U-TAE

Subsampling the satellite image time series is necessary for two main reasons:

- **Redundancy and noise in temporal observations.** There is currently no comprehensive study establishing the exact number of time steps required to classify crops reliably using U-TAE or other architectures. Existing works vary widely, for example, Garnot and Landrieu (2021) uses up to 61 observations, while Turkoglu et al. (2021a) employs 71 timestamps. In principle, Sentinel-2 can provide an observation every 2 to 3 days over Switzerland, making very long sequences feasible. However, such long sequences are often redundant and noisy: Metzger et al. (2021) reports that roughly 50% of observations can be unusable due to cloud cover. Moreover, crops may develop relatively slowly, e.g. in periods with low temperatures. Consequently, analogous to a slowly evolving video, densely sampling in time adds little new information for distinguishing crop types.

- **Computational efficiency and memory constraints.** Deep temporal models like U-TAE require substantial GPU memory when processing long sequences. To maintain a reasonable batch size during training, it is essential to limit the number of timestamps. Note that larger batches reduce the variance in the estimation of the gradient, resulting in a stronger and more stable training signal (Räisä et al., 2024). This is particularly advantageous for highly imbalanced datasets: choosing a batch size several times the minority-to-majority class ratio ensures that each minibatch contains sufficient minority-class examples to learn meaningful features (Google Developers, 2025).

To ensure our evaluation remains unbiased, we base our initial analysis on the well-established PASTIS benchmark, a concise and reproducible *toy* crop classification dataset introduced alongside U-TAE by Garnot et al. (2021). By mirroring SwissCrop’s multi-temporal structure while remaining fully independent, PASTIS enables rapid iteration and guarantees that insights from our analysis directly inform algorithm design without the dataset itself biasing the method.

In this dataset each time series contains on average 48 Sentinel-2 observations (up to 61). We uniformly subsampled each sequence to 24 time steps, and trained with a batch size of 4 (see Garnot and Landrieu (2021) for full training details). As shown in Table 1, this simple uniform subsampling yields only a 0.2% absolute drop in overall accuracy, despite no selective filtering of cloudy or low-information dates. Crucially, GPU memory usage is cut in half, and the number of multiply-accumulate operations (MACs) per forward pass with a single batch is reduced around 50%, dramatically lowering computational cost and freeing capacity for larger batches or faster training and inference. Accordingly, we set the temporal length to 24 for the experiments.

Table 1. Performance comparison for varying temporal length on the Pastis dataset. Results are averaged over a 5-fold experimental setting of the Pastis dataset. Refer to Garnot and Landrieu (2021) for details. M stands for GPU memory.

T_{min}	T_{max}	T_{mean}	M(Gb)	MACs(B)	Acc(%)
38	61	48	16.8	288	83.1 ± 0.5
24	24	24	8.0	145	82.9 ± 0.5

Positional encoding (PE) injects information about each observation’s position in the sequence into the attention mechanism, enabling the network to distinguish the order and spacing of time steps. In U-TAE, we add a standard PE, computed as a set of sinusoids at different frequencies, to the input embeddings to mark each time index. We experimented with alternative encodings that explicitly encode absolute time intervals rather than simple positional indices, but found no performance gain, indicating that U-TAE primarily leverages the relative ordering of observations rather than their exact timestamps (Figure 4).

Specifically, we trained three U-TAE variants with different position encodings:

- **noPE:** All position embeddings are set to zero.
- **linearPE:** Positions are encoded as sequential integers (1, 2, 3, ...).
- **calendarPE:** Positions are encoded as the actual calendar dates of each observation (1, ..., 365).

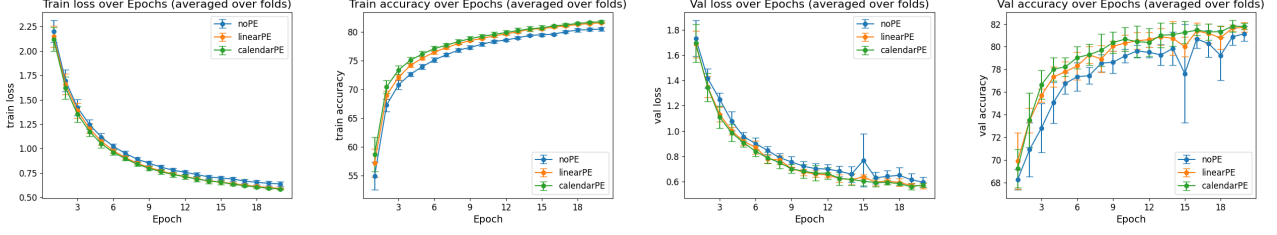


Figure 4. Learning curves of the U-TAE model with different position encodings (PE) on the PASTIS dataset, showing training loss, training accuracy, validation loss, and validation accuracy respectively.

As shown in Figure 4, the noPE model underperforms in both training and validation metrics, confirming that some ordering information is necessary. However, the linearPE and calendarPE models converge to nearly identical performance, suggesting that incorporating absolute time values (whether calendar dates or temperature-derived values) does not yield additional benefits beyond preserving the relative order of observations. This result led us to conclude that using thermal time directly as a positional encoding is unlikely to be very effective, as we show in our experiments.

In summary, our preliminary findings reveal that (i) substantial temporal subsampling incurs only a marginal accuracy loss while reducing both GPU memory usage and computational cost drastically, and (ii) U-TAE relies chiefly on the relative ordering of observations, whereas absolute timestamps offer limited benefit. These insights suggest that, rather than encoding raw dates, we should focus on selecting the most informative, developmentally relevant observations. In the next section, we leverage this principle to introduce model-agnostic approach that partitions input sequences according to growing degree days to better align sampling with crop physiology.

3.3 T3S: Thermal-Time-based Temporal Sampling

Satellite-based crop monitoring approaches often rely on fixed-interval calendar-day sampling to construct input sequences. However, this overlooks the ecophysiological processes of plant growth such as their dependence on temperature. As crop development is tightly coupled with temperature, we propose a simple yet effective model-agnostic sampling method, Thermal-Time-based Temporal Sampling (T3S), which replaces fixed calendar intervals with intervals defined in thermal time, using Growing Degree Days (GDD) as the temporal reference.

GDD provides a cumulative measure of heat accumulation, reflecting the physiological development of crops more faithfully than absolute time. For a given day d , GDD is computed as:

$$\text{GDD}_d = \max\left(0, \frac{T_{\max,d} + T_{\min,d}}{2} - T_{\text{base}}\right), \quad (1)$$

where $T_{\max,d}$ and $T_{\min,d}$ are the daily maximum and minimum temperatures, respectively, and T_{base} is a base threshold below which crop development is considered negligible. In our experiments, we use $T_{\text{base}} = 0^\circ\text{C}$, a commonly used value for temperate climate crops.

We then compute the cumulative GDD over time:

$$\text{GDD}_D = \sum_{d=1}^D \text{GDD}_d. \quad (2)$$

To construct a time series of L observations, we partition the full GDD range $[\text{GDD}_{\min}, \text{GDD}_{\max}]$ into L uniform intervals. Within each interval, we select the least cloudy satellite observation, prioritizing data quality. Importantly, Sentinel-2 products include a freely available cloud mask layer, allowing direct use of cloud information without additional preprocessing. This ensures that the selected timestamps correspond to ecophysiological meaningful intervals that are consistent across different years, even when calendar dates diverge significantly due to seasonal variability.

The T3S algorithm is outlined in Algorithm 1. It takes as input the full set of timestamps, the cumulative thermal time values, i.e. GDD, the satellite data cube, a cloud mask for each observation, and the desired number of samples L . For each thermal interval, it identifies candidate observations and selects the one with the fewest cloud-contaminated pixels. The final set of selected indices is sorted to preserve temporal order. Figure 5 illustrates the overall workflow of our approach.

This sampling method offers several advantages. First, it aligns input sequences more closely with crop development, reducing temporal noise caused by inter-annual climatic shifts. Second, it improves data efficiency by avoiding redundant or uninformative observations. Lastly, T3S is agnostic to model architecture and can be seamlessly integrated into any time series-based crop monitoring pipeline.

Algorithm 1 T3S

```

1: function T3S(timeStamps, GDD, data, cloudMask, L)
2:    $t_{\min} \leftarrow \min(\text{GDD})$ 
3:    $t_{\max} \leftarrow \max(\text{GDD})$ 
4:    $\Delta \leftarrow (t_{\max} - t_{\min})/L$  #L is target temporal length
5:    $\text{selected} \leftarrow []$ 
6:    $\text{current} \leftarrow t_{\min}$ 
7:   while  $|\text{selected}| < L$  and  $\text{current} < t_{\max}$  do
8:      $\text{next} \leftarrow \text{current} + \Delta$ 
9:      $\text{window} \leftarrow \{i \mid \text{current} \leq \text{GDD}[i] < \text{next}\}$ 
10:    if  $\text{window} \neq \emptyset$  then
11:       $\text{best} \leftarrow \arg \max_{i \in \text{window}} \sum (\text{cloudMask}[i] = 0)$ 
12:      append  $\text{best}$  to  $\text{selected}$ 
13:    end if
14:     $\text{current} \leftarrow \text{next}$ 
15:  end while
16:  sort( $\text{selected}$ )
17:  return  $\text{data}[:, \text{selected}, \dots]$ 
18: end function

```

3.4 Training Details

The model was trained for 100 epochs using a batch size of 8 and a fixed temporal length of 24. We employed the Adam

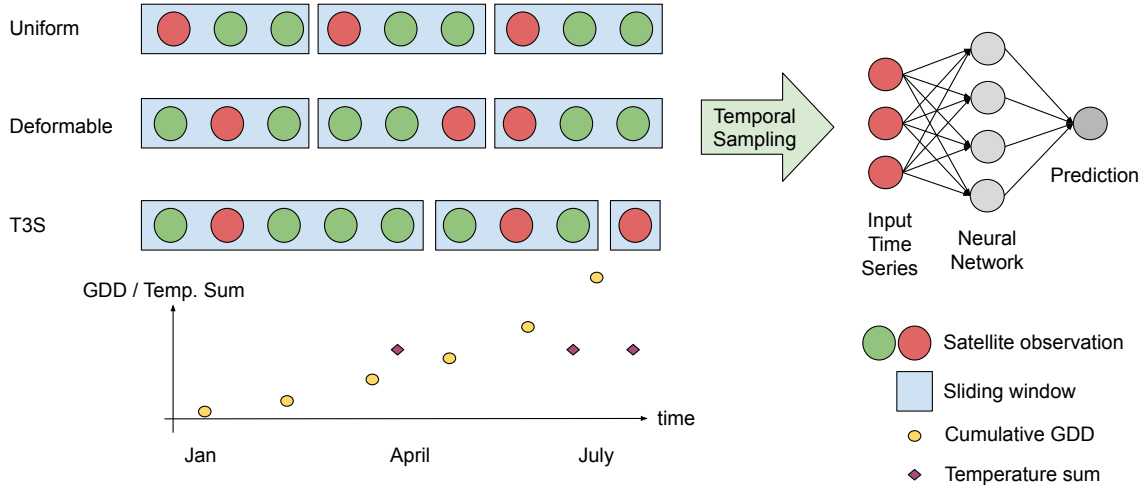


Figure 5. The first row shows conventional uniform sampling; the second row shows uniform sampling where the least cloudy observation is chosen in each interval (referred to as “Deformable” baseline); the third row shows the proposed Thermal-Time-based Temporal Sampling (T3S) approach. In T3S, each square box represents the temperature sum accumulated since the previous one, illustrating intervals with equal thermal time.

optimizer with an initial learning rate of 0.001, scheduled by a OneCycleLR policy with a maximum learning rate of 0.01 and a warm-up phase covering 30% of the total training steps. The U-TAE architecture is configured with an encoder having channel widths [128, 128, 128, 256], a symmetric decoder with widths [32, 64, 128, 256] and strided convolutions with kernel size $k = 4$, stride $s = 2$, and padding $p = 1$. The temporal attention module employs $n_{\text{head}} = 16$ heads and a model dimension of $d_{\text{model}} = 256$. Input features are standardized to zero mean and unit variance on a per-channel basis. We implemented the model in PyTorch and trained it on a single NVIDIA RTX 4090 GPU over roughly three days. The full codebase and pretrained checkpoints will be publicly available on GitHub.

4. Dataset

In this work, we work with **SwissCrop 2021, 2022, 2023**, a three-year crop dataset covering the entirety of Switzerland from 2021 to 2023. SwissCrop combines Sentinel-2 Level-2A bottom-of-atmosphere multi-spectral imagery with annual crop-type labels for each field. The dataset includes 50 distinct crop types, each representing the primary crop grown in a field during a given season. These labels were provided by farmers to the cantons of Switzerland according to a data model provided by the Federal Office for Agriculture¹ and joined together by the Swiss Centre for Agricultural Research, Agroscope. Unlike many existing datasets, e.g. Pastis dataset (Garnot and Landrieu, 2021), SwissCrop faithfully reflects the pronounced class imbalance found in real-world farming: a long-tail distribution in which a handful of major crops dominate while the majority occur only sporadically (cf. Figure 6).

The data is organized into analysis-ready data cubes optimized for deep learning applications (Figure 7). Each cube corresponds to a single year and covers a 128×128 pixel region (equivalent to 1280×1280 m at Sentinel-2’s 10 m resolution). We include the following spectral bands in each cube: B02 (Blue), B03 (Green), B04 (Red), B05 (Vegetation Red Edge1), B06 (Vegetation Red Edge2), B07 (Vegetation Red Edge3), B08 (Near-Infrared), B8A (Red Edge4), and B12 (Short-Wave Infrared2).

¹ <https://www.blw.admin.ch/de/landwirtschaftliche-kulturfleachen>

All imagery is reprojected to UTM zone 32N and resampled so that pixel coordinates align to a 10 m grid. In addition to optical bands, each cube stores the Scene Classification Layer (SCL), which provides both land-cover classification and cloud information. To minimize storage requirements, band values are saved as 16-bit integers (digital numbers), representing reflectance scaled by 10,000. Over the three years, SwissCrop comprises around 20K cubes per year, fully covering Switzerland’s agricultural area with consistent preprocessing and labeling. This dataset enables large-scale, cross-year experiments in crop classification and phenology analysis.

To complement these remote sensing observations, we incorporate high-resolution gridded climate data from MeteoSwiss, which supplies near-surface temperature fields (minimum, maximum, and average) on 1 km, 2 km, and 5 km grids (Federal Office of Meteorology and Climatology, MeteoSwiss, 2024). In our study, we use the 1 km daily minimum (TminD) and maximum (TmaxD) temperature series to compute growing degree days (GDD; refer to Section 3.3).

We make the full SwissCrop dataset publicly available to the research community. We hope this resource will facilitate further advances in large-scale, cross-year crop classification, phenology modeling, and earth observation research.

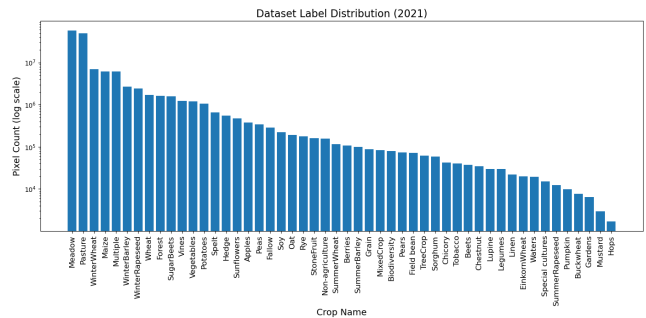


Figure 6. SwissCrop dataset label distribution for the year 2021. Note the logarithmic scale of the y-axis.

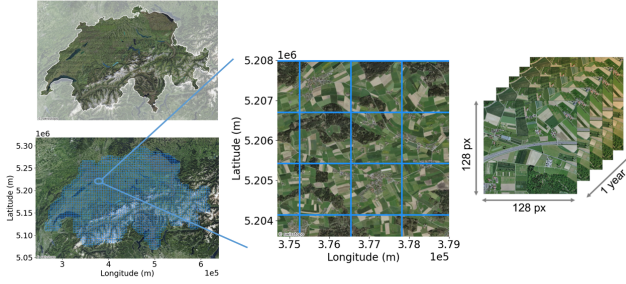


Figure 7. Region of interest (top left), the SwissCrop dataset (bottom left) and its coverage by data cubes (center), with an example of a single analysis-ready cube (right).

5. Experiment & Results

We evaluate the proposed T3S against four very relevant state-of-the-art baselines using a leave-one-year-out scheme over the 2021–2023 SwissCrop dataset. In each of six cross-year folds, two seasons are held out for testing while the remaining one season is used for training. To further assess robustness, we conduct a low-data experiment using only 10% of the labels, and an early-season study by truncating each test timeseries at the 50th and 75th time percentile (end of June and end of September respectively). We assess model predictive performance using *Overall accuracy*, the fraction of pixels correctly labeled; *Intersection-over-Union (IoU)*, the ratio of the area of overlap between predicted and ground-truth pixels to the area of their union; and *Mean Intersection-over-Union (mIoU)*, averaged across classes. Calibration is measured by the *Expected Calibration Error (ECE)*, which measures how far predicted confidences deviate from observed error rates, i.e., perfect calibration occurs when the estimated uncertainties match the actual likelihood of a misclassification. We also report *Negative Log-Likelihood (NLL)*, the mean negative log-probability of the true class, and the *Brier Score*, the mean squared error between predicted probabilities and one-shot labels.

Baselines. **U-TAE** is a U-Net combined with a temporal attention encoder (i.e., self-attention layer) that ingests images at fixed calendar dates and uses sinusoidal day-of-year positional encodings; it serves as our primary reference. We combine U-TAE with MC Dropout (Gal and Ghahramani, 2016): **U-TAE+MC-Dropout** retains the same sampling grid but activates dropout layers at test time to perform Monte Carlo sampling, thereby approximating a Bayesian posterior and yielding pixel-level uncertainty estimates without changing the input dates. Note that Monte Carlo Dropout remains one of the most popular and theoretically grounded methods for uncertainty calibration in deep learning (Kendall and Gal, 2017). Empirically, the number of ensemble members is set to 5, and the drop rate is set to 0.2. **U-TAE+Thermal-PE** follows Nyborg et al. (2022) and replaces the sinusoidal calendrical encodings with absolute thermal-time (Growing Degree Days) embeddings, giving the network explicit phenological context while still sampling on calendar dates. **U-TAE+Deformable Sampling** follows the same fixed-interval calendar schedule (e.g. one image per fifteen days) but “deforms” each interval by selecting the least-cloudy observation, thus reducing noise from clouds without altering the temporal grid.

Cross-Year Generalization and Uncertainty Calibration. T3S consistently outperforms all baselines in cross-year generalization (see Table 2), delivering an approximate 6% absolute improvement in overall accuracy over U-TAE, alongside gains in IoU and mean IoU. The discrepancy between IoU and mean IoU reflects the dataset’s long-tailed label distribution: rare classes contribute near-zero scores, pulling down the mean. Figure 8 shows that most crop categories benefit from T3S. Only the rarest classes (e.g., hop), for which both models lack sufficient training samples, remain at zero accuracy. Meadow accuracy drops slightly, reflecting U-TAE’s tendency to overpredict the dominant class and incur more false positives.

Crucially, T3S also yields much better-calibrated outputs. T3S reduces ECE by roughly fourfold compared to U-TAE, approaching perfect calibration, and substantially lowers both Negative Log-Likelihood and Brier Score, indicating sharper and more reliable uncertainty estimates. By comparison, U-TAE+MC-Dropout achieves the second-best calibration, modestly boosting accuracy and reducing ECE relative to vanilla U-TAE but still falling short of T3S. Note that MC-Dropout is specifically designed to improve the uncertainty calibration. U-TAE+Thermal-PE introduces phenological context via GDD embeddings and yields moderate gains in both performance and calibration, yet does not match the robustness of thermal-time sampling. Refer to Section 3.2 for a detailed analysis of its limited efficacy. Deformable Sampling improves predictive accuracy through cloud filtering but does so at the expense of uncertainty quality, exhibiting higher ECE. Overall, these results highlight that aligning observations by thermal time via temporal sampling, combined with cloud-aware selection yields the most robust and trustworthy cross-year crop mapping models.

Qualitative Comparison. Figure 11 contrasts T3S and U-TAE on both classification and uncertainty estimation, where pixel-wise uncertainty is defined as $1 - \max(\text{softmax}) \in [0, 1]$. In the first example, both models misclassify the highlighted region, but U-TAE remains overconfident in its incorrect label while T3S appropriately elevates uncertainty around the error. In the second example, T3S confines its errors to the fuzzy edges of the highlighted field, which is understandable given that farmers hand-draw plot boundaries and 10m pixels often cover two crop types, and its uncertainty map shows a pronounced hotspot exactly along those misclassified borders. In contrast, U-TAE not only mislabels the entire field but also produces a diffuse, misaligned uncertainty map that neither highlights its own errors nor respects the actual field geometry. In the third example, T3S again flags its error with a pronounced uncertainty hotspot, even revealing a likely ground-truth annotation mistake, while U-TAE provides no meaningful uncertainty signal. These examples illustrate that T3S not only reduces classification errors but also delivers well-calibrated uncertainty estimates that expose both model and dataset inconsistencies.

Low Data Regime. In many agricultural settings, annotated crop labels are scarce or expensive to obtain, which makes low data performance a critical requirement for operational viability. To assess robustness under label scarcity, we conducted a six-fold experiment using only 10 % of the training data, randomly sampled once and held constant across methods, and evaluated both T3S and U-TAE on the full test set. As shown in Figure 9, both models incur drops in accuracy and increases in Expected Calibration Error when labels are limited, but U-TAE’s performance deteriorates far more rapidly. Remarkably,

Table 2. Performance comparison across six evaluation settings. The first two columns show the year of the training and test datasets. Best score for each setting and each metric in **bold**, second best underlined.

Train	Test	Method	Accuracy % (↑)	mIoU % (↑)	IoU % (↑)	ECE (↓)	NLL (↓)	Brier Score (↓)
2021	2022	U-TAE (Garnot and Landrieu, 2021)	70.1	17.2	53.9	0.053	0.943	0.412
		+MC-Dropout (Gal and Ghahramani, 2016)	71.3	17.4	55.4	0.032	0.911	0.402
		+Thermal-PE (Nyborg et al., 2022)	72.5	18.6	56.9	0.045	0.854	0.385
		+Deformable Sampling	73.8	20.5	58.5	0.044	0.836	0.371
		T3S (ours)	76.0	21.6	61.3	0.004	0.720	0.329
2021	2023	U-TAE (Garnot and Landrieu, 2021)	71.4	16.7	55.6	0.052	0.947	0.399
		+MC-Dropout (Gal and Ghahramani, 2016)	72.5	17.0	56.8	0.037	0.918	0.394
		+Thermal-PE (Nyborg et al., 2022)	71.3	15.5	55.4	0.035	0.925	0.401
		+Deformable Sampling	74.6	18.9	59.6	0.032	0.822	0.359
		T3S (ours)	77.6	21.0	63.5	0.005	0.691	0.307
2022	2021	U-TAE (Garnot and Landrieu, 2021)	70.8	16.2	54.8	0.035	0.936	0.408
		+MC-Dropout (Gal and Ghahramani, 2016)	71.2	16.2	55.3	0.024	0.913	0.399
		+Thermal-PE (Nyborg et al., 2022)	72.8	18.2	57.2	0.077	1.022	0.403
		+Deformable Sampling	76.8	20.4	62.3	0.043	0.833	0.339
		T3S (ours)	77.3	<u>20.1</u>	63.0	0.013	0.697	0.310
2022	2023	U-TAE (Garnot and Landrieu, 2021)	72.1	17.4	56.4	0.041	0.875	0.389
		+MC-Dropout (Gal and Ghahramani, 2016)	72.8	17.2	57.2	0.028	0.853	0.381
		+Thermal-PE (Nyborg et al., 2022)	63.9	14.2	46.9	0.123	1.374	0.525
		+Deformable Sampling	<u>76.0</u>	<u>20.8</u>	<u>61.4</u>	0.073	0.936	<u>0.363</u>
		T3S (ours)	76.8	20.9	62.4	0.019	0.708	0.318
2023	2021	U-TAE (Garnot and Landrieu, 2021)	71.6	17.6	55.8	0.066	0.913	0.398
		+MC-Dropout (Gal and Ghahramani, 2016)	71.6	17.6	55.7	0.040	0.889	<u>0.391</u>
		+Thermal-PE (Nyborg et al., 2022)	71.8	16.3	56.0	0.098	0.987	0.413
		+Deformable Sampling	75.3	20.5	60.4	0.105	0.951	0.379
		T3S (ours)	77.1	23.2	62.8	0.019	0.686	0.307
2023	2022	U-TAE (Garnot and Landrieu, 2021)	71.2	18.4	55.3	0.059	0.957	0.410
		+MC-Dropout (Gal and Ghahramani, 2016)	72.0	18.6	56.2	0.043	0.929	0.400
		+Thermal-PE (Nyborg et al., 2022)	75.3	19.6	60.4	0.085	0.929	0.366
		+Deformable Sampling	<u>75.8</u>	<u>21.9</u>	<u>61.0</u>	0.081	<u>0.827</u>	<u>0.355</u>
		T3S (ours)	76.9	22.3	62.5	0.006	0.687	0.311
Average		U-TAE (Garnot and Landrieu, 2021)	71.2 ± 0.6	17.3 ± 0.7	55.3 ± 0.8	0.051 ± 0.012	0.929 ± 0.028	0.403 ± 0.008
		+MC-Dropout (Gal and Ghahramani, 2016)	71.9 ± 0.6	17.3 ± 0.7	56.1 ± 0.7	0.034 ± 0.007	0.902 ± 0.029	0.395 ± 0.007
		+Thermal-PE (Nyborg et al., 2022)	71.3 ± 3.5	17.1 ± 1.9	55.5 ± 4.1	0.077 ± 0.029	1.015 ± 0.156	0.416 ± 0.053
		+Deformable Sampling	<u>75.4 ± 1.0</u>	<u>20.5 ± 0.9</u>	<u>60.5 ± 1.2</u>	0.063 ± 0.025	<u>0.868 ± 0.045</u>	<u>0.361 ± 0.014</u>
		T3S (ours)	77.0 ± 0.5	21.5 ± 1.0	62.6 ± 0.7	0.011 ± 0.006	0.698 ± 0.012	0.314 ± 0.008

T3S trained on just 10 % of the data still outperforms U-TAE trained on the full dataset, and its calibration remains substantially more reliable.

This advantage stems from the incorporation of a meaningful inductive bias, namely the thermal time prior, which encodes domain knowledge about crop development into the model architecture. By constraining the hypothesis space to reflect biologically plausible growth patterns, T3S requires fewer examples to learn robust representations, making it far more data efficient and noise resilient, for example, against cloud cover and sensor artifacts, than models trained purely in a data-driven fashion. These results demonstrate that thermal time inductive bias confers strong resilience to small data scenarios, underscoring T3S’s practicality for real-world applications where labels are limited. See Section 6 for more discussion.

Early-Season Classification. Early season classification is an important aspect of this technology, since some applications require crop labeling during the growing season rather than after harvest. To evaluate T3S in this context, we truncate the test set time series at two percentiles, 75 percent (end of September) and 50 percent (end of June), and perform a six fold experiment in which both T3S and U-TAE are trained on full-season data and tested on the truncated series. Figure 10 shows that both models experience a decline in in-season performance, measured by predictive accuracy and uncertainty estimation, when using partial time series. At the 75 percent cutoff, U-TAE’s performance drops sharply, whereas T3S remains virtually unchanged. Moreover, at the 50 percent cutoff, T3S attains a similar level of accuracy and uncertainty calibration that U-TAE achieves using the full season of data. These results indicate that T3S not only improves in-season classification accuracy and uncertainty quantification but also underscores its practical suitability for operational in-season crop monitoring and

decision-support applications, where timely and reliable predictions are critical.

6. Discussion

Our experiments demonstrate that embedding GDD-informed sampling into a deep learning pipeline not only improves crop classification accuracy but also yields better-calibrated uncertainty estimates compared to leading baselines. This advantage grows when training data are scarce, highlighting the value of domain expertise under low-data regimes.

Injecting domain knowledge into a neural network, i.e., inductive bias, constrains the hypothesis space to solutions that ‘make sense’ under known physical or biological rules and this prevents the model from assigning high confidence to predictions when evidence is weak or contradictory (Mitchell (1980), Ahmadi Daryakenari et al. (2024)). In our case inductive bias is introduced via GDD-informed sampling. By incorporating thermal time alignment, we align satellite time series with actual crop phenology. This inductive bias acts as a regularizing prior, steering the model toward meaningful growth stages and away from noisy or cloud-contaminated observations. As a result, high-confidence predictions coincide with clear phenological cues, while lower-confidence outputs correctly signal uncertainty, demonstrating reliable probability calibration.

By combining deep neural networks with agronomic expertise, our approach not only enhances classification accuracy but also empowers the model to recognize and flag its own uncertainty, an essential feature in agricultural decision-making, where misplaced confidence can have costly consequences.

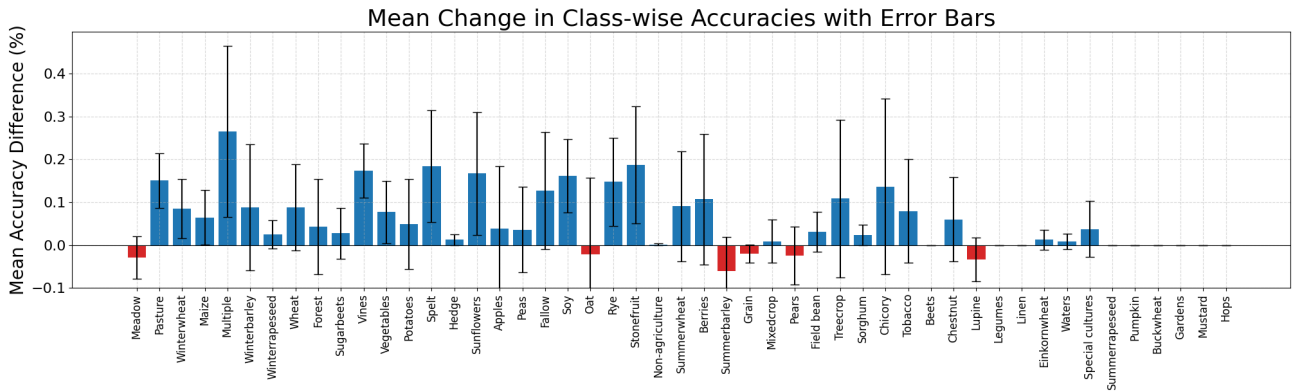


Figure 8. Class-wise accuracy difference between the proposed T3S and U-TAE. Averaged over six experimental folds. Blue bars indicate classes where T3S outperforms U-TAE, while red bars indicate classes where T3S underperforms.

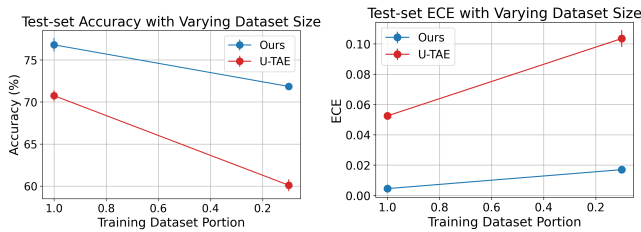


Figure 9. Low data regime performance showing classification (a) accuracy and (b) Expected Calibration Error averaged over six folds when training on 10% of the data, comparing T3S (Ours) and U-TAE.

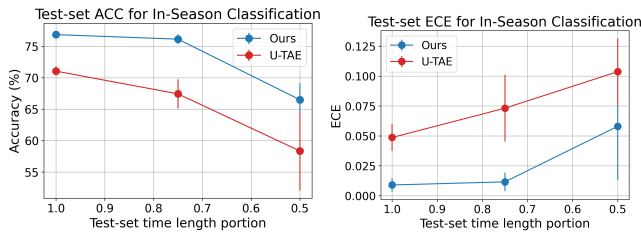


Figure 10. In-season classification performance at the 75th- and 50th-percentile cutoffs, corresponding to the end of September and the end of June, respectively, showing (a) accuracy and (b) Expected Calibration Error, averaged over six folds, for T3S (Ours) versus U-TAE.

7. Conclusion

In this paper, we introduced Thermal Time-based Temporal Sampling (T3S), a simple, model-agnostic method that uses cumulative growing degree days to select relevant observations within satellite time series for crop growth-related applications. Based on basic ecophysiological principles of crop growth, it reduces the computational load by removing redundant information and allows to prioritize relevant and undisturbed imagery. Although we evaluated T3S with attention-based deep learning architecture, it can be seamlessly integrated with any machine learning model. When compared to other state-of-the-art approaches, T3S not only enhances predictive accuracy but also markedly improves uncertainty estimation, an aspect often overlooked in the literature. Furthermore, we made evaluation on SwissCrop, a novel, large-scale, multi-year dataset spanning three growing seasons (2021–2023) across Switzerland’s agricultural landscapes, thereby providing a real-world benchmark for compared methods. By releasing both SwissCrop and our

T3S implementation to the public, we establish a robust, reproducible benchmark for the community, facilitating fair comparisons and driving further innovation in crop-growth modelling. For future work, incorporating additional environmental drivers such as precipitation could further strengthen temporal alignment and robustness across diverse agro-climatic regions.

8. Declaration of Competing Interest

The authors declare that they have no known competing financial interests or personal relationships that could have appeared to influence the work reported in this paper.

9. Acknowledgments

Mehmet Ozgur Turkoglu acknowledges support from Agroscope through research funding for the CropMAIpper project. Sélène Ledain acknowledges funding from the Swiss Federal Office of Agriculture and Agroscope within the Monitoring of the Swiss Agri-Environmental System (MAUS) program. This project was conducted in the context of the Swiss Agricultural Landscape Intelligence platform, funded through an Agroscope Research grant awarded to Helge Aasen.

References

- Ahmadi Daryakenari, N., De Florio, M., Shukla, K., Karniadakis, G. E., 2024. AI-Aristotle: A physics-informed framework for systems biology gray-box identification. *PLOS Computational Biology*, 20(3), e1011916.
- Bai, S., Zhang, Z., Ding, M., Liu, Y., Chen, C., Ghanem, B., 2023. ViTs for SITS: vision transformers for satellite image time series. *arXiv preprint*.
- Baumert, J., Heckeley, T., Storm, H., 2024. Probabilistic crop type mapping for ex-ante modelling and spatial disaggregation. *Ecological Informatics*, 83, 102836.
- Becker, A., Russo, S., Puliti, S., Lang, N., Schindler, K., Wegner, J. D., 2023. Country-wide retrieval of forest structure from optical and SAR satellite imagery with deep ensembles. *ISPRS Journal of Photogrammetry and Remote Sensing*, 195, 269–286.
- Blickensdörfer, L., Schwieder, M., Pflugmacher, D., Nendel, C., Erasmí, S., Hostert, P., 2022. Mapping of crop types

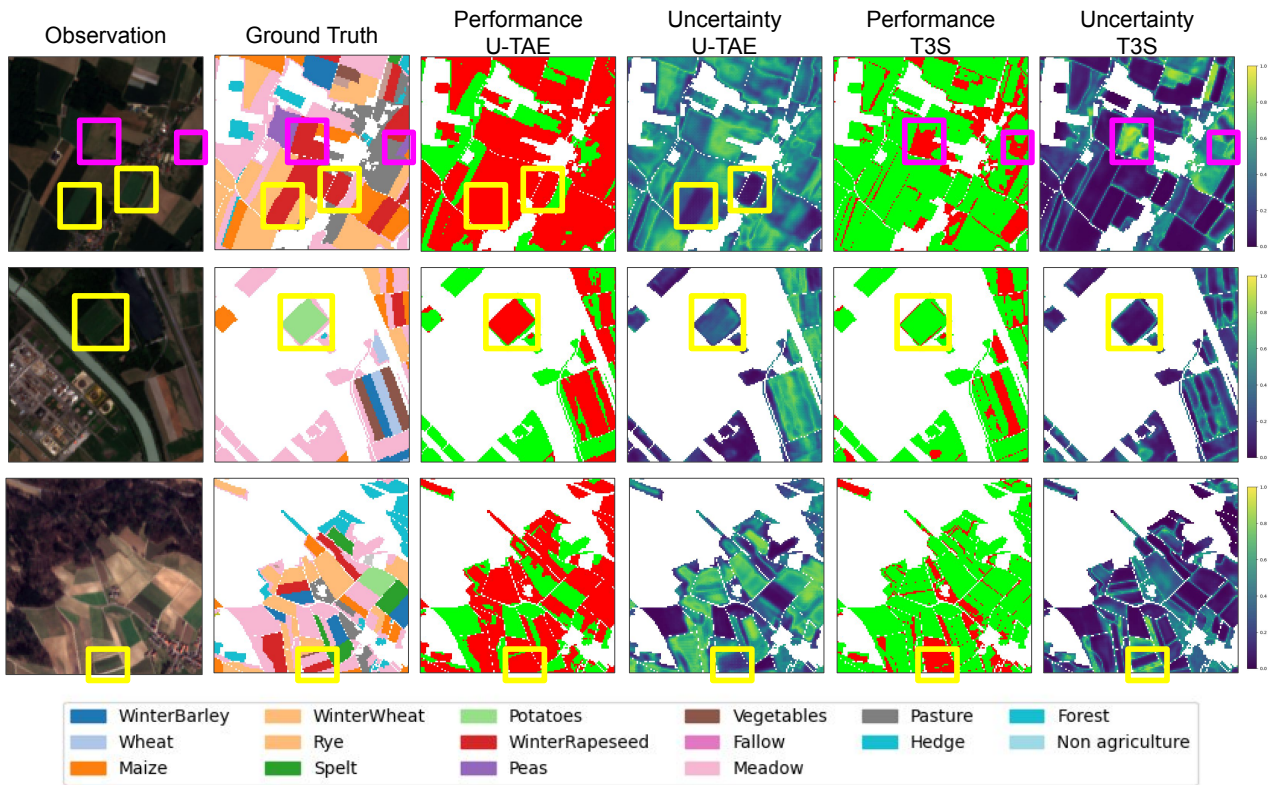


Figure 11. Qualitative comparison for the proposed T3S and U-TAE. In performance maps, red indicates a wrong prediction while green represents a correct prediction. High uncertainty is indicated by yellow, while low is indicated with dark blue.

and crop sequences with combined time series of Sentinel-1, Sentinel-2 and Landsat 8 data for Germany. *Remote sensing of environment*, 269, 112831.

Blundell, C., Cornebise, J., Kavukcuoglu, K., Wierstra, D., 2015. Weight uncertainty in neural networks. *International Conference on Machine Learning (ICML)*, 1613–1622.

Cai, X., Bi, Y., Nicholl, P., Sterritt, R., 2023. Revisiting the encoding of satellite image time series. *arXiv preprint arXiv:2305.02086*.

Chen, T., Guestrin, C., 2016. Xgboost: A scalable tree boosting system. *Proceedings of the 22nd ACM SIGKDD International Conference on Knowledge Discovery and Data Mining*, ACM, 785–794.

Dubrovin, K., Verkhoturov, A., Stepanov, A., Aseeva, T., 2024. Multi-Year Cropland Mapping Based on Remote Sensing Data: A Case Study for the Khabarovsk Territory, Russia. *Remote Sensing*, 16(9), 1633.

Durasov, N., Bagrov, A., Vetrov, D., 2021. Masksembles for uncertainty estimation. *Proceedings of the IEEE/CVF Conference on Computer Vision and Pattern Recognition (CVPR)*, 13539–13548.

Federal Office of Meteorology and Climatology, MeteoSwiss, 2024. The climate of Switzerland.

Gal, Y., Ghahramani, Z., 2016. Dropout as a bayesian approximation: Representing model uncertainty in deep learning. *International Conference on Machine Learning (ICML)*, 1050–1059.

Gao, Z., Guo, D., Ryu, D., Western, A. W., 2023. Training sample selection for robust multi-year within-season crop classification using machine learning. *Computers and Electronics in Agriculture*, 210, 107927.

Garnot, V. S. F., Landrieu, L., 2021. Panoptic segmentation of satellite image time series with convolutional temporal attention networks. *Proceedings of the IEEE/CVF International Conference on Computer Vision*, 4872–4881.

Garnot, V. S. F., Landrieu, L., Giordano, S., Chehata, N., 2020. Satellite image time series classification with pixel-set encoders and temporal self-attention. *Proceedings of the IEEE/CVF Conference on Computer Vision and Pattern Recognition*, 12325–12334.

Gómez, C., White, J. C., Wulder, M. A., 2016. Optical remotely sensed time series data for land cover classification: A review. *ISPRS Journal of Photogrammetry and Remote Sensing*, 116, 55–72.

Google Developers, 2025. Imbalanced datasets. Machine Learning Crash Course. Accessed June 2025.

Gustafsson, F. K., Danelljan, M., Schön, T. B., 2019. Evaluating scalable bayesian deep learning methods for robust computer vision. *CVPR Workshops*, 318–319.

Huang, G., Li, Y., Pleiss, G., Liu, Z., Hopcroft, J. E., Weinberger, K. Q., 2017. Snapshot ensembles: Train 1, get m for free. *International Conference on Learning Representations (ICLR)*.

Kendall, A., Gal, Y., 2017. What uncertainties do we need in bayesian deep learning for computer vision? *Advances in neural information processing systems*, 30.

- Khallaghi, S., Abedi, R., Ali, H. A., Alemohammad, H., Asipunu, M. D., Alatise, I., Ha, N., Luo, B., Mai, C., Song, L. et al., 2025. Generalization enhancement strategies to enable cross-year cropland mapping with convolutional neural networks trained using historical samples. *Remote Sensing*.
- Lakshminarayanan, B., Pritzel, A., Blundell, C., 2017. Simple and scalable predictive uncertainty estimation using deep ensembles. *Advances in Neural Information Processing Systems (NeurIPS)*, 6402–6413.
- Lang, N., Jetz, W., Schindler, K., Wegner, J. D., 2022. A high-resolution canopy height model of the Earth. *Nature*, 608, 259–264.
- Li, G., Han, W., Dong, Y., Zhai, X., Huang, S., Ma, W., Cui, X., Wang, Y., 2023. Multi-year crop type mapping using sentinel-2 imagery and deep semantic segmentation algorithm in the Hetao Irrigation District in China. *Remote Sensing*, 15(4), 875.
- Liu, Y., Diao, C., Mei, W., Zhang, C., 2024. CropSight: Towards a large-scale operational framework for object-based crop type ground truth retrieval using street view and Planet-Scope satellite imagery. *ISPRS Journal of Photogrammetry and Remote Sensing*, 216, 66–89.
- Maleki, R., Wu, F., Oubara, A., Fathollahi, L., Yang, G., 2024. Refinement of Cropland Data Layer with Effective Confidence Layer Interval and Image Filtering. *Agriculture*, 14(8), 1285.
- Metzger, N., Turkoglu, M. O., D’Aronco, S., Wegner, J. D., Schindler, K., 2021. Crop classification under varying cloud cover with neural ordinary differential equations. *IEEE Transactions on Geoscience and Remote Sensing*, 60, 1–12.
- Mitchell, T. M., 1980. The need for biases in learning generalizations.
- Mühlematter, D. J., Halbheer, M., Becker, A., Narnhofer, D., Aasen, H., Schindler, K., Turkoglu, M. O., 2024. LoRA-Ensemble: Efficient Uncertainty Modelling for Self-attention Networks. *arXiv preprint arXiv:2405.14438*.
- Nyborg, J., Pelletier, C., Assent, I., 2022. Generalized classification of satellite image time series with thermal positional encoding. *Proceedings of the IEEE/CVF Conference on Computer Vision and Pattern Recognition*, 1392–1402.
- Qi, H., Qian, X., Shang, S., Wan, H., 2024. Multi-year mapping of cropping systems in regions with smallholder farms from Sentinel-2 images in Google Earth engine. *GIScience & Remote Sensing*, 61(1), 2309843.
- Qin, X., Su, X., Zhang, L., 2024. SITSMamba for Crop Classification based on Satellite Image Time Series. *arXiv preprint arXiv:2409.09673*.
- Räsä, O., Jälkö, J., Honkela, A., 2024. Subsampling is not magic: Why large batch sizes work for differentially private stochastic optimisation. *arXiv preprint arXiv:2402.03990*.
- Ronneberger, O., Fischer, P., Brox, T., 2015. U-net: Convolutional networks for biomedical image segmentation. *Medical image computing and computer-assisted intervention—MICCAI 2015: 18th international conference, Munich, Germany, October 5-9, 2015, proceedings, part III 18*, Springer, 234–241.
- Roscher, R., Russwurm, M., Gevaert, C., Kampffmeyer, M., Dos Santos, J. A., Vakalopoulou, M., Hänsch, R., Hansen, S., Nogueira, K., Prexl, J., Tuia, D., 2024. Better, Not Just More: Data-centric machine learning for Earth observation. *IEEE Geoscience and Remote Sensing Magazine*, 12(4), 335–355.
- Rußwurm, M., Courty, N., Emonet, R., Lefèvre, S., Tuia, D., Tavenard, R., 2023. End-to-end learned early classification of time series for in-season crop type mapping. *ISPRS Journal of Photogrammetry and Remote Sensing*, 196, 445–456.
- Rußwurm, M., Körner, M., 2017. Temporal vegetation modelling using long short-term memory networks for crop identification from medium-resolution multi-spectral satellite images. *Proceedings of the IEEE Conference on Computer Vision and Pattern Recognition Workshops*.
- Rußwurm, M., Körner, M., 2018. Multi-temporal land cover classification with sequential recurrent encoders. *ISPRS International Journal of Geo-Information*, 7(4), 129.
- Rußwurm, M., Körner, M., 2020. Self-attention for raw optical satellite time series classification. *ISPRS Journal of Photogrammetry and Remote Sensing*, 169, 421–435.
- Rußwurm, M., Lefèvre, S., Körner, M., 2019. Breizhcrops: A satellite time series dataset for crop type identification. *ICML Workshop*.
- Sainte Fare Garnot, V., Landrieu, L., 2020. Leveraging Class Hierarchies with Metric-Guided Prototype Learning. *arXiv preprint arXiv:2007.03047*.
- Schneider, M., Schelte, T., Schmitz, F., Körner, M., 2023. Eurocrops: The largest harmonized open crop dataset across the european union. *Scientific Data*, 10(1), 612.
- Series, T., 2020. Lightweight temporal self-attention for classifying satellite images. *Advanced Analytics and Learning on Temporal Data: 5th ECML PKDD Workshop, AALTD 2020, Ghent, Belgium, September 18, 2020, Revised Selected Papers*, 12588, Springer Nature, 171.
- Sykas, D., Sdraka, M., Zografakis, D., Papoutsis, I., 2022. A sentinel-2 multiyear, multicountry benchmark dataset for crop classification and segmentation with deep learning. *IEEE Journal of Selected Topics in Applied Earth Observations and Remote Sensing*, 15, 3323–3339.
- Tarasiou, M., Chavez, E., Zafeiriou, S., 2023. Vits for sits: Vision transformers for satellite image time series. *Proceedings of the IEEE/CVF Conference on Computer Vision and Pattern Recognition*, 10418–10428.
- Tian, H., Wang, P., Tansey, K., Wang, J., Quan, W., Liu, J., 2024. Attention mechanism-based deep learning approach for wheat yield estimation and uncertainty analysis from remotely sensed variables. *Agricultural and Forest Meteorology*, 356, 110183.
- Turkoglu, M. O., 2023. Deep learning for vegetation classification from optical satellite image time series. PhD thesis, ETH Zurich.
- Turkoglu, M. O., Aasen, H., Schindler, K., Wegner, J. D., 2024a. Country-wide cross-year crop mapping from optical satellite image time series. Technical report, Copernicus Meetings.

Turkoglu, M. O., Becker, A., Gündüz, H. A., Rezaei, M., Bischl, B., Daudt, R. C., D’Aronco, S., Wegner, J. D., Schindler, K., 2022. FiLM-Ensemble: Probabilistic deep learning via feature-wise linear modulation. *Advances in Neural Information Processing Systems*.

Turkoglu, M. O., D’Aronco, S., Perich, G., Liebisch, F., Streit, C., Schindler, K., Wegner, J. D., 2021a. Crop mapping from image time series: deep learning with multi-scale label hierarchies. *arXiv preprint arXiv:2102.08820*.

Turkoglu, M. O., D’Aronco, S., Wegner, J. D., Schindler, K., 2021b. Gating revisited: Deep multi-layer RNNs that can be trained. *IEEE Transactions on Pattern Analysis and Machine Intelligence*, 44(8), 4081–4092.

Turkoglu, M. O., D’Aronco, S., Schindler, K., Wegner, J. D., 2024b. Hierarchical Crop Mapping from Satellite Image Sequences with Recurrent Neural Networks. *Multitemporal Earth Observation Image Analysis: Remote Sensing Image Sequences*, 41.

Vaswani, A., Shazeer, N., Parmar, N., Uszkoreit, J., Jones, L., Gomez, A. N., Kaiser, Ł., Polosukhin, I., 2017. Attention is all you need. *Advances in Neural Information Processing Systems (NeurIPS)*.

Weiss, M., Jacob, F., Duveiller, G., 2020. Remote sensing for agricultural applications: A meta-review. *Remote sensing of environment*, 236, 111402.

Welling, M., Teh, Y. W., 2011. Bayesian learning via stochastic gradient langevin dynamics. *International Conference on Machine Learning (ICML)*, 681–688.

Xie, E., Wang, W., Yu, Z., Anandkumar, A., Alvarez, J. M., Luo, P., 2021. SegFormer: Simple and efficient design for semantic segmentation with transformers. *Advances in neural information processing systems*, 34, 12077–12090.